









Cite this: *Digital Discovery*, 2025, 4, 2244

Automated electron microscopy sample preparation system†

David Milsted, ^{‡a} Tara P. Mishra, ^{‡a} Lauren N. Walters, ^{bc} Yuxing Fei, ^{ab} Bernardus Rendy, ^{ab} Pragnay Nevatia, ^d Haegyeom Kim ^a and Gerbrand Ceder ^{*ab}

The emergence of self-driving laboratories (SDLs) promises to innovate chemistry and materials science by incorporating autonomous systems for experimental design and execution. Advanced material characterization techniques, such as electron microscopy, are crucial for determining the materials synthesized by SDLs, and integrating these techniques into the SDL workflow is of paramount importance. Despite recent advancements, automated preparation of samples for electron microscopy remains challenging due to the specialized and hard-to-replicate human processes involved in powder dispensing and sample transfer. In this work, we introduce an automated electron microscopy sample preparation robot (EMSBot) that is designed for the preparation of powder samples for electron microscopy in SDLs. To enable easy integration with existing SDL hardware and software, EMSBot is equipped with a user-friendly interface and a modular design. Beyond automating this traditionally manual process, EMSBot delivers more consistent and higher-quality powder dispersions compared to conventional manual preparation. As a result, EMSBot streamlines sample preparation and accelerates the integration of advanced multiscale characterization techniques such as scanning and transmission electron microscopy into existing SDL workflows.

Received 22nd March 2025
Accepted 8th July 2025

DOI: 10.1039/d5dd00116a

rsc.li/digitaldiscovery

Computational and high-throughput materials investigations have paved the way for accelerated discovery and prediction of materials with unique properties.^{1–5} The experimental realization of these predicted materials, aimed at increasing experimental throughput, has been advanced by the development of self-driving laboratories (SDLs). Driven by high-performance computing, customizable hardware development, and machine learning, SDLs hold great promise in augmenting efficiency in experimental protocols.^{6,7} Additionally, SDLs have promoted the reproducibility and digitization of research in experimental materials.⁸ While SDLs have successfully automated the synthesis of thin films,^{9–11} solution-based synthesis,¹² nanoparticle synthesis,¹³ and solid-state materials,^{14,15} advanced material characterization remains a critical component for determining experimental outcomes and providing essential feedback to these systems.

To address this, researchers have made substantial progress in automating various characterization techniques, both within and outside the SDL framework. These advances include optical and electron microscopy,^{16,17} X-ray diffraction, and even the automation of experiments at large-scale facilities such as synchrotrons.¹⁸ Parallel developments in autonomous algorithms have improved the analysis of complex datasets obtained from electron microscopy^{19–21} and X-ray diffraction.^{22,23} The advent of benchtop scanning electron microscopes (SEMs), such as the PhenomXL and SNE-Alpha, has broadened access to morphology and compositional characterization of novel materials at the micron scale within SDLs. Furthermore, integrating data from electron microscopy with other techniques, such as X-ray diffraction, can provide richer insights for autonomous algorithms, ultimately enhancing the capabilities of SDLs.²⁴

Despite these advancements, integrating advanced characterization techniques, particularly electron microscopy, continues to present significant challenges. One primary obstacle is the lack of reproducible and automated sample preparation methods. This issue is especially pronounced in research and development environments, where sample preparation platforms must accommodate diverse material systems while maintaining sufficient adaptability for integration into existing characterization instruments without degrading the integrity of the samples.

^aMaterials Science Division Lawrence Berkeley National Laboratory, Berkeley, CA 94720, USA. E-mail: gceder@berkeley.edu^bDepartment of Materials Science and Engineering, University of California Berkeley, Berkeley, CA 94720, USA^cBakar Institute of Digital Materials for the Planet, University of California Berkeley, Berkeley, CA 94720, USA^dDepartment of Chemical Engineering, University of California Berkeley, Berkeley, CA 94720, USA† Electronic supplementary information (ESI) available. See DOI: <https://doi.org/10.1039/d5dd00116a>

‡ These authors contributed equally to this work.



Traditional scanning electron microscopy (SEM) sample preparation of inorganic materials typically involves drop-casting a small amount of powder onto a stub covered with carbon or copper tape, followed by removing excess material using an air blower or by gently tapping the stub on a hard surface.^{25–28} These steps require precise and delicate manual manipulation of very small quantities of material, making them difficult to replicate with robotic systems. Additionally, manual drop-casting can lead to significant particle agglomeration, especially with challenging samples, which complicates downstream autonomous analysis such as particle size determination. These limitations hinder the reliable integration of SEM sample preparation into SDL ecosystems.

Manual transmission electron microscopy (TEM) sample preparation presents its own challenges, typically requiring particles of less than 100 nm in thickness. Achieving this often involves mechanically grinding powder samples, dissolving them in a non-reactive solvent, sonication, and subsequent dispersion onto a TEM grid.²⁹ Although these procedures can yield suitably sized particles for characterization, they are labor-intensive and involve complex manual steps that are difficult to automate. While some progress has been made in automating TEM sample preparation, such as using focused ion beam (FIB) technology³⁰ or automating the preparation of biological specimens,^{31,32} automated procedures for preparing inorganic powder samples remain lacking.

Therefore, there is a pressing need for modular, automated systems capable of preparing powder samples for both SEM and TEM, thereby facilitating material characterization within SDL workflows.

To address this gap, we introduce “EMSBot”, a solvent-free automated modular device designed specifically for electron microscopy powder sample preparation in SDLs. EMSBot leverages static electricity principles, utilizing induced opposing charges between the powder particles and electron microscopy sample holders (SEM stubs or TEM grids) to achieve controlled particle deposition. This system offers unique advantages, including seamless integration with existing SDLs and the ability to facilitate individual user requests through a browser-based graphical user interface (GUI). Furthermore, this toolkit presents the versatility to prepare samples for both scanning electron microscopy (SEM) and transmission electron microscopy (TEM) within a single setup. Notably, EMSBot exhibits change in particle size dispersion based on operating conditions, allowing for the potential preferential deposition of smaller particles onto either TEM grids or SEM stubs. EMSBot addresses the critical challenge of automated powder sample preparation, paving the way for the integration of advanced electron microscopy techniques into autonomous inorganic solid-state materials research workflows.

1 Experimental methods

1.1 Mechanical design of EMSBot

EMSBot is composed of two main components: a customized 3D printer (Fig. 1A and B) and a control panel (ESI Fig. S1 and S2†). The 3D printer is a modified Creality Ender3 Pro with

a BigTreeTech SKR Mini E3 V2.0 motherboard. All objects were designed using CAD software and printed with PLA filament. The original printer nozzle head is replaced with a custom “handling robot” (Fig. 1C) designed to hold needles for picking up SEM stubs and TEM grids. The main components of the handling robot are shown in Fig. 1C.

The printer bed is replaced with a 5 mm-thick polypropylene bed to provide electrical insulation. Custom 3D-printed objects such as the SEM stub tray (Fig. 1E) and TEM grid tray (Fig. 1D) are assembled on this bed. The parts of the SEM stub tray are shown in Fig. 1E. The bot is equipped with a removable tray (E1), allowing easy replacement to bring in clean stubs when necessary.

Similarly, the parts of the TEM grid tray are shown in Fig. 1D. A laser sensor (D2) is installed to verify that the handling robot has picked up a SEM stub or a TEM grid for the exposition of the powder sample. The stepper motor (D3) uncovers the TEM grid tray (D8) by lifting the original TEM grid lid (D7) using a stainless steel sheet (D6) attached to the lid and a magnet (D5) attached to the pivoting cover (D4). The lid in the TEM grid is crucial to prevent cross-contamination between the clean TEM grids and powder sample deposited grids.

On the polypropylene bed, a custom 3D-printed sample exposition station (Fig. 1F) is assembled. This station is used to place the container containing the powder sample for deposition onto the SEM or TEM grids. The parts of the sample exposition system are marked in Fig. 1F. The enclosure (F3) secures the sample container, allowing the electrode (F5) to touch the bottom of the container.

The handling bot constitutes a vacuum system, controlled by the control panel, which includes two vacuum pumps connected to the SEM and TEM needles in the handling robot. This system enables the handling robot to pick up a SEM stub or a TEM grid for sample preparation for electron microscopy. While vacuum is a common method for picking TEM grids, it is not standard for SEM stubs.

Particle deposition onto the SEM stub and TEM grids is based on electrostatic attraction. A Spellman SL30P300 high-voltage power supply (HVPS) provides the required voltage and current as specified by the control panel. The distribution and interconnection diagram of the control panel is shown in ESI Fig. S2.† The handling robot uses a vacuum pump to pick up the sample holders. The SEM electrode wire connects to the SEM needle (C3), which attracts the sample powders. The TEM electrode is a live wire placed about 3 mm above the picked grid, enhancing the electrical field strength above the grid. The TEM needle (C4) is made of plastic, with the electrode wire shaped to form a sharp point to attract the sample powders through the TEM grid.

EMSBot is controlled using a Python-based backend, allowing remote control through socket requests (for integration with an SDL), or through a webpage for human-machine interface front-end (ESI Fig. S3–S5†).

1.2 Experimental testing of EMSBot

To analyze the powder samples prepared using the EMSBot we undertook SEM characterization using a benchtop Phenom XL



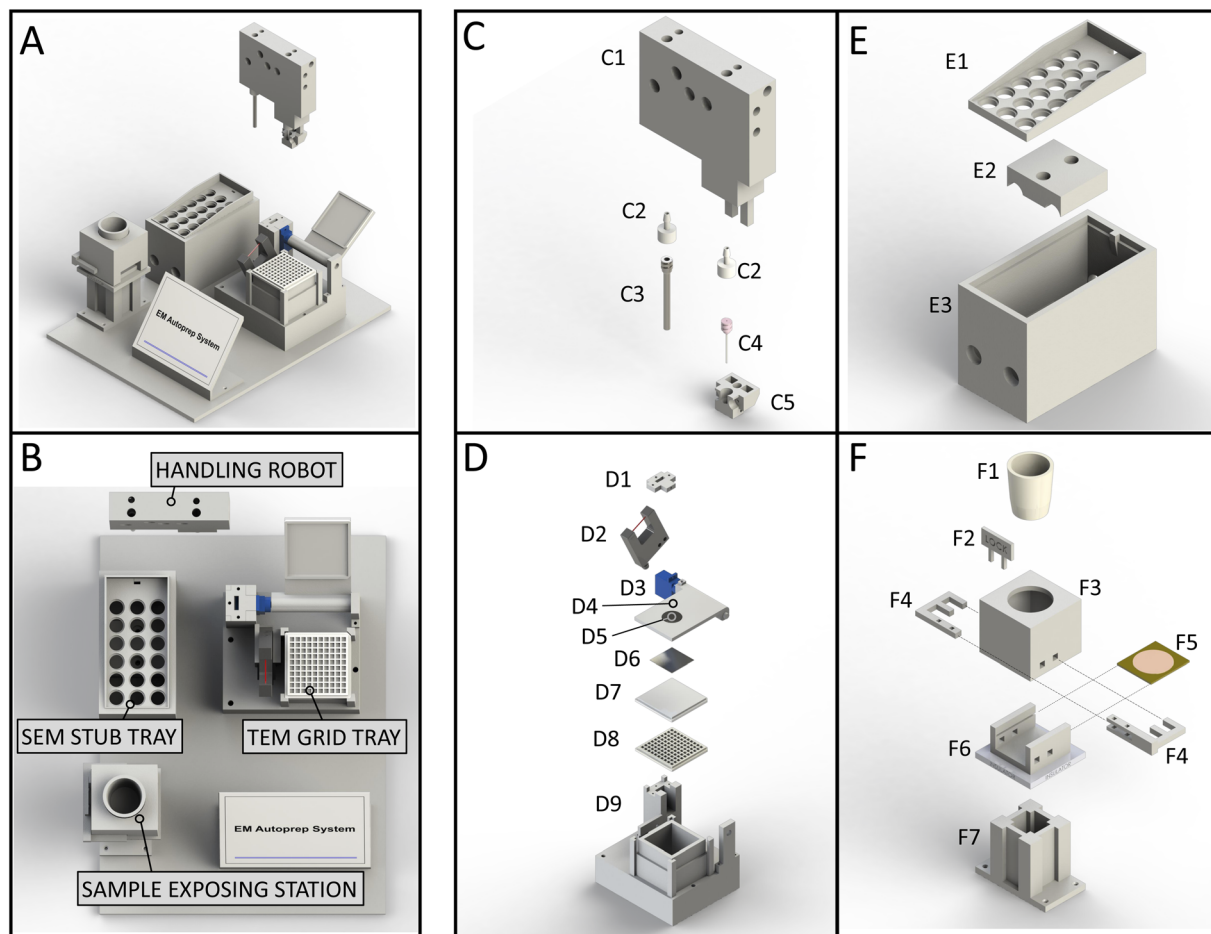


Fig. 1 Design of EMSBot. (A) 3D and (B) top overview of the components of the EMSBot. (C) Parts of the handling robot with the main structural body (C1), luer lock hose adaptors (C2), 8G stainless steel blunt needle (C3), 22G PTFE blunt needle (C4), wire positioner and plastic needle support (C5). (D) Parts of the TEM grid tray with the motor holder (D1), laser sensor (D2), stepper motor (D3), pivoting cover (D4), 20 mm Ø flat magnet (D5), 20 × 20 mm stainless steel sheet (D6), TEM tray lid (D7), TEM grid tray (D8), and main structural body (D9). (E) SEM stub tray with removable stud tray (E1), hose holder (E2), and main structural body (E3). (F) Sample exposition system with the sample holder (F1), electrical enclosure lock A (F2), electrical enclosure cover (F3), electrical enclosure lock B (F4), field-emitting area (F5), electrical enclosure support (F6), and main structural body (F7).

G2 desktop SEM. The SEM samples were prepared utilizing SEM stubs mounted with carbon tape. Powder samples were prepared using a constant electrostatic voltage of 10 kV and a current of 10 mA for 5 seconds. TEM samples were prepared using a standard 3.05 mm diameter formvar supported copper grids, with deposition parameters of 10 kV and 10 mA and 5 seconds of hold time. STEM-HAADF characterization was carried using a FEI TitanX 60-300 microscope housed at National Center for Electron Microscopy at the Molecular Foundry at the Lawrence Berkeley National Laboratory.

2 Results

2.1 Working schematic of EMSBot

The sample preparation procedure starts with a set of SEM stubs (Fig. 1(E1)) or TEM grid trays (Fig. 1(D8)), and a container containing the powder is placed in the sample exposition station either by a robot or a user (Fig. 1(F1)). The sample

preparation steps EMSBot follows are shown algorithmically in Fig. 2, with a detailed control flow diagram in ESI Fig. S6.† The operation commands for the EMSBot can be provided either by the user or automatically by an SDL operating system such as AlabOS.³³ A video of the EMSBot operation is available in ESI Video 1.†

The instructions for sample preparation involves selecting if a SEM stub or if a TEM grid will be prepared, and then determining the distance of the SEM stub or TEM grid from the powder sample surface, setting the electric field voltage, and specifying the exposition time. The handling bot picks up the relevant stub or grid and verifies the task's success using a laser sensor. If the bot fails to pick up the holder, it attempts the task three times before generating an error message that requires human assistance. Once the sample holder is successfully picked up, the handling bot transfers it to the exposition station, where powder samples are deposited onto the grid or stub using the electrostatic method according to the exposition



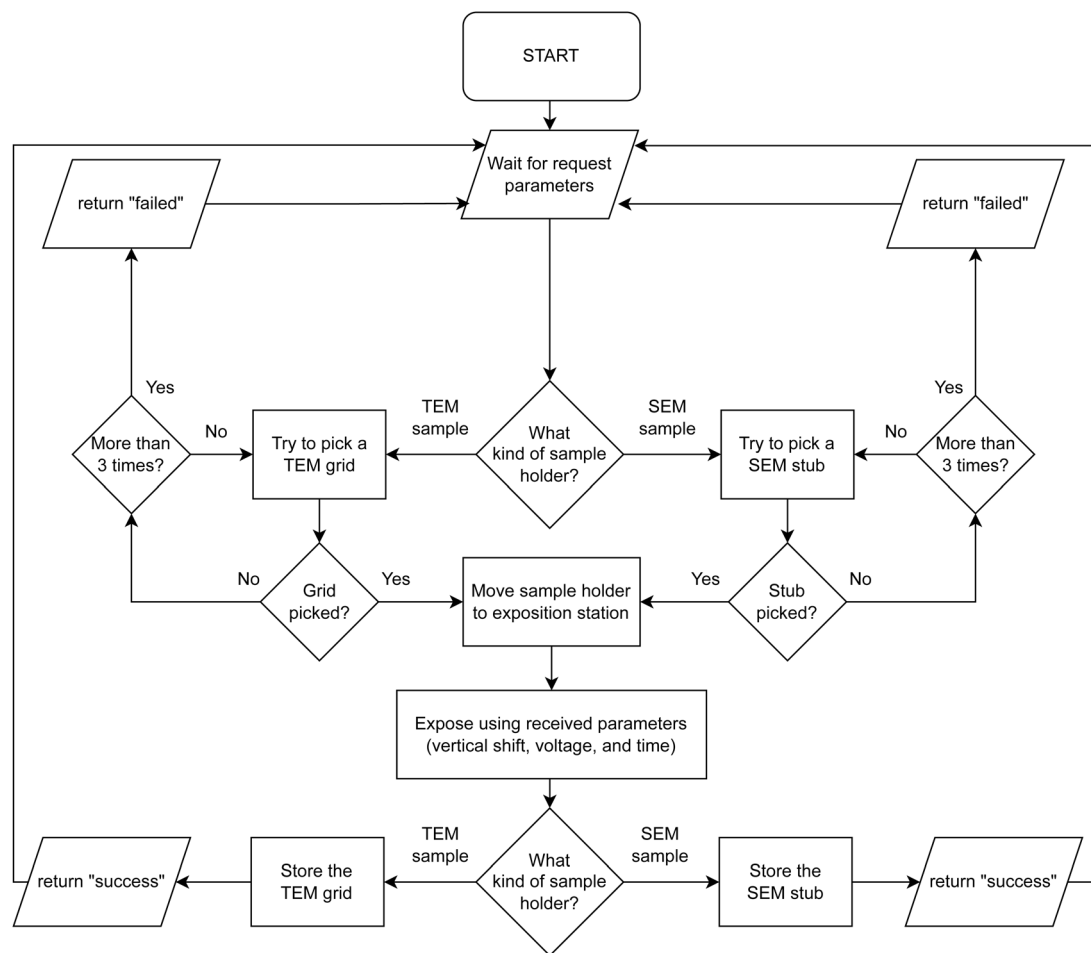


Fig. 2 Flow chart depicts the operation algorithm of EMSBot.

parameters. After deposition, the SEM stub or TEM grid is returned to the sample storage area, and a success message is sent to the controller, indicating readiness for the next round of powder sample preparation.

2.2 Experimental verification of the working of EMSBot

To evaluate the quality of the powder samples prepared by the EMSBot into SEM stubs and TEM grids, we conducted SEM and TEM characterization of these samples. Given the possible variability of sample height within the crucible, we measured the position of the SEM stub relative to the top rim of the crucible during sample transfer, as shown schematically in Fig. 3A. Fig. 3B presents typical low magnification SEM micrographs of samples acquired by placing the SEM stub at 15 mm (top panel) and 20 mm (bottom panel) below the top rim of the crucible, illustrating the dispersion of $\text{Al}(\text{OH})_3$ particles transferred onto the SEM stub using the EMSBot.

The position of the stub with reference to the top rim of the crucible is an easily controllable parameter during the sample preparation using the EMSBot. Hence, it is interesting to note the effect of the stub position on the sizes of the collected particles. To statistically analyze the dispersion of particle sizes in the sample prepared using the EMSBot, multiple SEM

micrographs at different stub positions were analyzed. The particles were identified in the SEM micrographs through a thresholding procedure followed by binarization. These binary maps were then used to calculate the area of each particle. This analysis was performed using the ImageJ software.³⁴ The statistical distribution of particle areas at two positions, -15 mm and -20 mm from the top of the crucible on the SEM stub, is illustrated in the form of a histogram in Fig. 2C. A total of 314 and 868 particles over multiple stubs were statistically analyzed following the procedure above at these distances, respectively. Additional histograms for particle size distributions at SEM stub distances of -16 mm and -18 mm are provided in ESI Fig. S7.† From the histogram distribution, we observe that when the SEM stub is positioned further away from the powder surface (-15 mm from the top of the crucible), smaller particles are deposited. However, as the stub is systematically brought closer to the particle surface, both smaller and larger particles are deposited on the SEM stub. For example, when the stub is -15 mm from the top of the crucible, approximately 91% of the particles have an area less than $50 \mu\text{m}^2$, whereas at -20 mm, about 85% of the particles are less than $50 \mu\text{m}^2$. Additionally, a considerable percentage of the particles ($\approx 4\%$) are more than $200 \mu\text{m}^2$ when the stub is -20 mm from the top of the crucible. These results show



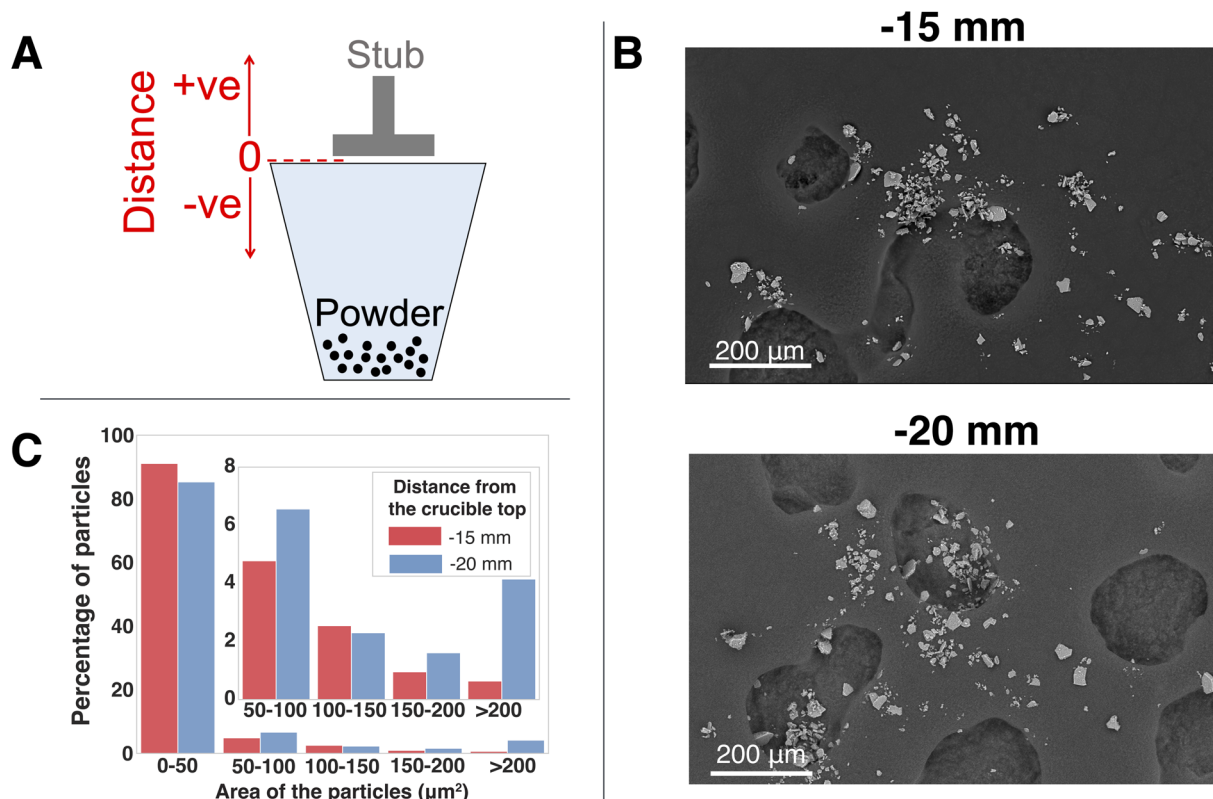


Fig. 3 Statistical analysis of the size of the particles prepared using EMSBot from SEM micrographs. (A) Convention of distance parameter followed during the exposition of the SEM stub/TEM grid. Typical SEM micrographs used for statistical analysis of the particle sizes were prepared from a distance of (A) –15 mm and (B) –20 mm from the top of the crucible rim. (C) Histogram analysis of the particle size as a function of the stub distance from the top of the crucible. (inset) Magnified histogram of the distribution of the particles >25 μm.

a change in particle size distribution upon the operating conditions of the EMSBot.

To demonstrate the uniformity of particle dispersion achieved with EMSBot-prepared samples, we compared SEM micrographs of samples prepared using both EMSBot and manual methods. Fig. 4 displays ball-milled precursor samples of $\text{Na}_4\text{P}_2\text{O}_7$ and SnO_2 , with EMSBot-prepared samples shown in panels A and B, and manually prepared samples in panels C and D. This particular precursor powder system was selected as a test case due to the challenges associated with manual SEM sample preparation and the importance of accurate particle size characterization for achieving the desired target composition, as previously highlighted by our group.³⁵

The SEM images clearly show that EMSBot-prepared samples (panel A) exhibit a more uniform particle distribution and greater separation between particles, whereas manually prepared samples (panel C) display significant agglomeration. Binary masked images derived from the SEM micrographs, shown in panels B (EMSBot) and D (manual), further emphasize these differences in particle dispersion. These binary masked images were used to determine the particle size distribution, as shown in ESI Fig. S8.†

Furthermore, to demonstrate the reproducibility of enhanced particle dispersion, we compared wet-mixed precursor samples of $\text{Na}_4\text{P}_2\text{O}_7$ and SnO_2 prepared using

EMSBot and manual methods. As shown in ESI Fig. S9,† EMSBot-prepared samples exhibit much better dispersion than manually prepared samples. The decrease in particle

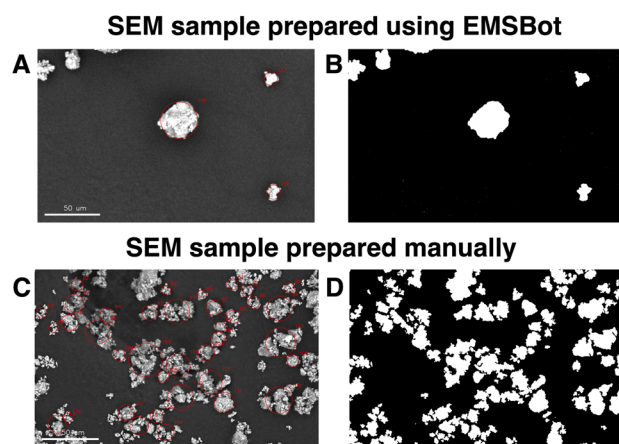


Fig. 4 Representative SEM images and corresponding segmentation masks used for particle size distribution analysis. Samples were prepared using EMSBot (A and B) and manual methods (C and D), with the examples depicting medium-sized particles (8–50 μm diameter). Left panels show SEM images with overlaid red circles and identification numbers indicating particles detected by the automated program. Right panels display the associated masks generated by image segmentation. The white bar denotes a scale of 50 μm.



agglomeration is also evident in the optical images presented in ESI Fig. S10.†

Overall, these results demonstrate that well-dispersed SEM stubs, as produced by EMSBot, enable more reliable particle size analysis by minimizing particle overlap compared to manually prepared stubs.

As illustrated in Fig. 1 and described in the associated text, another unique feature of the EMSBot is its ability to prepare samples for both scanning and transmission electron microscopy. For transmission electron microscopy sample preparation, a conventional TEM grid can be used instead of the SEM stub.

To demonstrate this capability, we prepared a TEM sample from $\text{Al}(\text{OH})_3$ powder using exposure parameters of 10 kV and 10 mA for 5 seconds, with the sample positioned 8 mm below the top of the crucible. A standard 3 mm holey carbon-supported copper (Cu) TEM grid was employed for sample collection. Fig. 5A presents a representative low-magnification scanning transmission electron microscope high-angle

annular dark field (STEM-HAADF) micrograph of $\text{Al}(\text{OH})_3$ particles. Well-dispersed electron-transparent particles, approximately 50 nm in diameter, are readily observed on the grid prepared using EMSBot, one example of which is highlighted in Fig. 5B.

To demonstrate the universality of the EMSBot in preparing powder samples for electron microscopy characterization, we prepared SEM samples of various materials, and the SEM micrographs of these samples are shown in Fig. 6. We tested oxide ceramics such as $\text{Na}_6\text{W}_{12}\text{O}_{39}$ and SiO_2 , hydroxides such as $\text{Ni}(\text{OH})_2$, phosphates such as $\text{NH}_4\text{H}_2\text{PO}_4$, metal particles such as Ti, carbonates such as Na_2CO_3 , and chlorides such as KCl. Furthermore, we also tested mixtures of particles such as Ti and Na_2CO_3 , and SiO_2 with Ti and KCl. In all of these cases, we were able to obtain an appreciable amount of well-dispersed particles for SEM characterization. Furthermore, to demonstrate the successful transfer of the different samples onto the SEM stub, SEM-EDS images are presented in ESI Fig. S11–S19.†

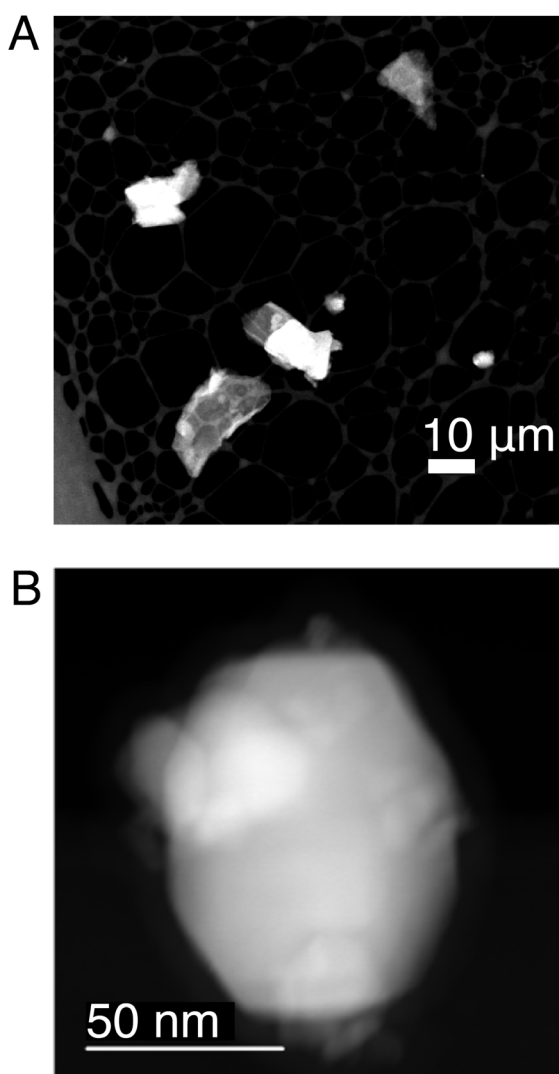


Fig. 5 Typical STEM-HAADF micrographs at different magnifications from a TEM grid prepared using the EMSBot sample preparation robot are shown, with (A) displaying a low-magnification micrograph and (B) presenting a high-magnification view of a representative particle.

3 Discussion

The creation of fully automated SDLs requires systems that are seamlessly integrated with one another across aspects of experimental procedures. Automated sample preparation has posed a critical bottleneck in integrating advanced characterization techniques such as electron microscopy into SDLs.⁶ In this work, we introduce EMSBot, which represents a significant advancement in the realm of automated electron microscopy powder sample preparation.

One of the most compelling advantages of EMSBot is its modular architecture, which enhances the adaptability of the system to various research environments while aligning with the objectives of incremental integration into mature autonomous labs. Research groups can incorporate EMSBot without extensive changes to their current systems, minimizing disruption and maximizing resource utilization. This integration is facilitated by a range of carefully engineered features on both the hardware and software fronts.

On the backend, EMSBot employs the UDP protocol to provide a robust programmatic interface for machine control.³⁶ The UDP server enables bi-directional communication between the client, such as a user or an autonomous lab orchestration system, and the EMSBot server. Given that most workflow orchestration systems utilize Python as the backend, researchers can implement a UDP client to establish communication with EMSBot, regardless of their operating system. UDP's platform independence, running over ethernet, ensures cross-platform compatibility. Furthermore, the EMSBot web server backend is built using Python, Flask, and SocketIO, widely adopted frameworks that can be deployed across diverse environments. To further streamline integration, EMSBot offers a set of clearly defined and well-documented APIs for controlling and monitoring the instrument. These APIs are documented in the source code, enabling research groups to rapidly develop adapter layers that integrate EMSBot with their workflow management and data storage systems. This approach mirrors the integration of commercial equipment, such as the



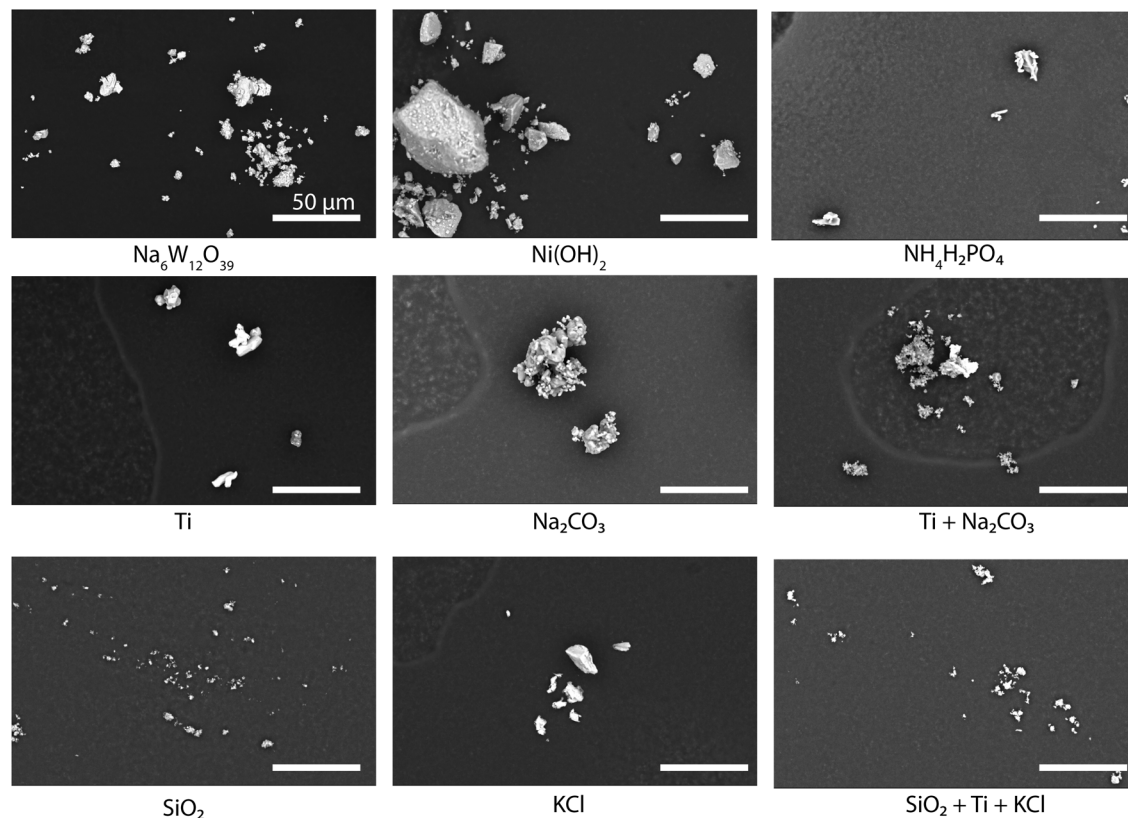


Fig. 6 SEM micrographs of various chemical compounds and powder mixtures prepared using the EMSBot. The white bar denotes a scale of 50 μm .

Mettler–Toledo balance, where adapters leverage standardized interfaces. Given the diversity of autonomous research platforms, including autonomous lab operating systems such as AlabOS, ChemOS 2.0, and HELAO, it is not feasible to provide ready-to-use integration code for every system.^{33,37,38} Instead, EMSBot's clean and accessible API allows users to readily adapt the integration to their specific workflows.

The hardware design of EMSBot also supports modularity and ease of integration. The sample input position, SEM stub holder, and TEM grid are all strategically placed on the bed to ensure collision-free access, particularly in coordination with mechanical manipulators such as robot arms. The stepper motor on the bed can move samples linearly with high accuracy (well below 1 mm) in the x - y plane, positioning them precisely where a manipulator can safely and efficiently transfer them to other systems. Additionally, the slotted aluminum extrusion frame allows the EMSBot to be securely mounted such as against an optical breadboard, ensuring consistent positioning over time.

The graphical user interface (GUI) and full Python backend serve as significant assets in this integration process, lowering the entry barrier for new users (ESI Fig. S3–S5†). Furthermore, the flexible hardware design anticipates the straightforward addition of standard powder sample preparation practices, such as mechanical grinding of particles, ensuring that EMSBot can evolve alongside the needs of the research community.

Statistical analyses conducted during our experiments reveal intriguing insights into the change in the particle size

distribution facilitated by the EMSBot. The distribution of particle sizes demonstrates that when the stub is positioned further away from the powder surface, primarily smaller particles are dispensed onto it, while a closer stub position allows both larger and smaller particles to be collected. This change in particle size distribution capability opens exciting new avenues for electron microscopy sample preparation. For instance, when preparing samples for Transmission Electron Microscopy (TEM) or techniques requiring strict particle size criteria, this feature could ensure that only appropriately sized particles are transferred to the specimen grids. However, further investigations need to be conducted to optimize the exposition criteria for samples with different chemistries and particle sizes to achieve particle size selectivity using EMSBot.

Samples prepared (ESI Fig. S9–S17†) by EMSBot can be analyzed using SEM-EDS to assess morphology and composition. Additionally, TEM grids produced with EMSBot are suitable for a wide range of advanced electron microscopy techniques, including electron diffraction. While particle size does not determine material chemistry, it plays a crucial role in characterization. Specifically, TEM measurements often require small particles (typically <150 nm) to achieve electron transparency, whereas SEM measurements generally necessitate larger particles (>200 nm) due to spatial resolution constraints. By enabling the preparation of appropriately sized powder samples, EMSBot effectively facilitates and supports



downstream characterization using both SEM and TEM for advanced analyses.

Samples prepared using the EMSBot show a uniform particle dispersion and significantly reduced particle agglomeration compared to the samples prepared manually (Fig. 4 and ESI S8–S10†). We hypothesize this uniformity is a result of the electrostatic repulsion between the charged particles during the transfer from the crucible to the SEM stub. Given that techniques such as micro electron diffraction (microED) necessitate a minimum separation of particles, typically greater than 1 μm for effective structure determination,³⁹ EMSBot's precision in controlling the quantity and size of particles could be invaluable in structure determination for new material systems. Furthermore, as previously demonstrated by our group, achieving phase purity of certain target phases may depend on the particle sizes of the precursors.³⁵ Uniform dispersion and reduced agglomeration of particles facilitate more accurate characterization of particle size by improving the reliability of particle-finding algorithms. Descriptors such as particle size, and its influence on achieving the target phase, can lead to better optimization of material synthesis recipes and provide valuable insights into synthesis science.

Another advantage of EMSBot is the solvent free approach to TEM sample preparation. Traditional drop-casting methods for TEM sample preparation often involve a solvent-based method for dispersing smaller particles in a dilute concentration and drop casting a small amount of the dispersed solution onto a TEM grid.^{40,41} However, in an SDL with a target of accelerated development of new materials, the stability of the synthesized material against solvents would be unknown, making TEM sample preparation challenging. While drop casting is a preferred pathway for many samples, it can also introduce artifacts for nanoparticles tending to agglomerate and dry up at the edge of the drop, leading to “coffee ring” effects.^{41,42} EMSBot overcomes these challenges by using static electricity for TEM sample preparation and provides an alternative solvent-free TEM sample preparation method for the SDL ecosystem.

Furthermore, our results demonstrate that EMSBot is effective across a broad range of material compositions, including oxides, hydroxides, halides, and pure metals, rendering the system material-agnostic for electron microscopy sample preparation (Fig. 6 and ESI S11–S19†). However, we identify limitations when working with materials that are highly hygroscopic or exhibit strong adhesion to the synthesis crucible, resulting in specimens that no longer remain in powder form. Notably, these limitations are similar to those encountered with manually prepared samples.

Finally, EMSBot is engineered to enable the preparation of both SEM and TEM samples within a single unit. While the integration of benchtop SEMs into self-driving laboratory (SDL) workflows has enhanced capabilities for composition and topography analysis,^{16,43–45} advanced characterization, such as electron diffraction from transmission electron microscopes, remains indispensable for new material discovery. However, due to time and cost constraints, it is not feasible to analyze every sample using TEM. To address this, we envision SDLs that can automatically flag promising novel material systems for

further investigation, with EMSBot automating the preparation of TEM specimens. This streamlines advanced characterization and fosters more efficient exploration of material properties.

4 Summary and conclusions

Powder sample preparation for advanced characterization techniques like SEM and TEM has been a significant bottleneck in adapting these methods into SDLs. In this work, we introduce EMSBot, an automated electron microscopy sample preparation robot that uses electrostatic dispersion of particles onto SEM stubs or TEM grids. EMSBot's modular design, intuitive GUI, and better dispersion of particles in the prepared samples contribute to increased throughput, improved reliability of analyses, and the facilitation of advanced characterization techniques in autonomous laboratories. Additionally, EMSBot employs a solution-free electron microscopy powder sample preparation system, making it particularly relevant for the electron microscopy characterization of environmentally sensitive samples. By automating the sample preparation procedures, EMSBot can help bridge advanced characterization into SDLs, ultimately accelerating discoveries in materials science by enabling more sophisticated experimental approaches and analyses.

Data availability

The EMSBot control panel diagram and data supporting this article have been included as part of the ESI.† The code for EMSBot is available at <https://github.com/dmilsted/EMSBot>. It is a part of alab_control package available at https://github.com/CederGroupHub/alab_control. The version used in this study is v1.0.0 and is available in the alab_control package as a release (1.1.0 – EMSBot). The version is also available at Zenodo repository at <https://doi.org/10.5281/zenodo.15866072>.

Conflicts of interest

There are no conflicts to declare.

Acknowledgements

The authors would like to thank Jiahao “Robert” Yao and Yuhan “Alex” Chen for their important help and support in developing the EMSBot as a part of their undergraduate projects. The authors would like to thank Arian Gashi for help with CNC machining of insulating parts and William Waldron for providing the power supply used in the project. This work was primarily supported by the Data-Drive Synthesis Science Core Program at Lawrence Berkeley National Laboratory under contact No. DE-AC02-05-CH11231. This work was also supported by the Laboratory Directed Research and Development Program of Lawrence Berkeley National Laboratory under U.S. Department of Energy Contract No. DE-AC02-05CH11231. Work at the Molecular Foundry was supported by the Office of Science, Office of Basic Energy Sciences, of the US DOE under



contract number DE-AC02-05CH11231. L.No..W. acknowledges funding support from the BIDMaP Postdoctoral Fellowship.

Notes and references

- 1 J. Schmidt, M. R. Marques, S. Botti and M. A. Marques, *npj Comput. Mater.*, 2019, **5**, 83.
- 2 K. Choudhary, B. DeCost, C. Chen, A. Jain, F. Tavazza, R. Cohn, C. W. Park, A. Choudhary, A. Agrawal, S. J. Billinge, *et al.*, *npj Comput. Mater.*, 2022, **8**, 59.
- 3 A. Jain, S. P. Ong, G. Hautier, W. Chen, W. D. Richards, S. Dacek, S. Cholia, D. Gunter, D. Skinner, G. Ceder, *et al.*, *APL Mater.*, 2013, **1**, 1.
- 4 A. Jain, G. Hautier, C. J. Moore, S. P. Ong, C. C. Fischer, T. Mueller, K. A. Persson and G. Ceder, *Comput. Mater. Sci.*, 2011, **50**, 2295–2310.
- 5 A. Jain, K. A. Persson and G. Ceder, *APL Mater.*, 2016, **4**, 1–14.
- 6 M. Abolhasani and E. Kumacheva, *Nat. Synth.*, 2023, **2**, 483–492.
- 7 G. Tom, S. P. Schmid, S. G. Baird, Y. Cao, K. Darvish, H. Hao, S. Lo, S. Pablo-García, E. M. Rajaonson, M. Skreta, *et al.*, *Chem. Rev.*, 2024, **124**, 9633–9732.
- 8 R. L. Greenaway, K. E. Jelfs, A. C. Spivey and S. N. Yaliraki, *Nat. Rev. Chem.*, 2023, **7**, 527–528.
- 9 B. P. MacLeod, F. G. Parlane, T. D. Morrissey, F. Häse, L. M. Roch, K. E. Dettelbach, R. Moreira, L. P. Yunker, M. B. Rooney, J. R. Deeth, *et al.*, *Sci. Adv.*, 2020, **6**, eaaz8867.
- 10 A. G. Kusne, H. Yu, C. Wu, H. Zhang, J. Hattrick-Simpers, B. DeCost, S. Sarker, C. Oses, C. Toher, S. Curtarolo, *et al.*, *Nat. Commun.*, 2020, **11**, 5966.
- 11 S. B. Harris, A. Biswas, S. J. Yun, K. M. Roccapiore, C. M. Rouleau, A. A. Puretzky, R. K. Vasudevan, D. B. Geohegan and K. Xiao, *Small Methods*, 2024, 2301763.
- 12 B. Burger, P. M. Maffettone, V. V. Gusev, C. M. Aitchison, Y. Bai, X. Wang, X. Li, B. M. Alston, B. Li, R. Clowes, *et al.*, *Nature*, 2020, **583**, 237–241.
- 13 Y. Jiang, D. Salley, A. Sharma, G. Keenan, M. Mullin and L. Cronin, *Sci. Adv.*, 2022, **8**, eabo2626.
- 14 N. J. Szymanski, B. Rendy, Y. Fei, R. E. Kumar, T. He, D. Milsted, M. J. McDermott, M. Gallant, E. D. Cubuk, A. Merchant, *et al.*, *Nature*, 2023, **624**, 86–91.
- 15 J. Chen, S. R. Cross, L. J. Miara, J.-J. Cho, Y. Wang and W. Sun, *Nat. Synth.*, 2024, 1–9.
- 16 Y. Liu, K. Roccapiore, M. Checa, S. M. Valleti, J.-C. Yang, S. Jesse and R. K. Vasudevan, *Small Methods*, 2024, 2301740.
- 17 S. V. Kalinin, D. Mukherjee, K. Roccapiore, B. J. Blaiszik, A. Ghosh, M. A. Ziatdinov, A. Al-Najjar, C. Doty, S. Akers, N. S. Rao, *et al.*, *npj Comput. Mater.*, 2023, **9**, 227.
- 18 D. Allan, T. Caswell, S. Campbell and M. Rikitin, *Synchrotron Radiat. News*, 2019, **32**, 19–22.
- 19 S. V. Kalinin, M. Ziatdinov, J. Hinkle, S. Jesse, A. Ghosh, K. P. Kelley, A. R. Lupini, B. G. Sumpter and R. K. Vasudevan, *ACS Nano*, 2021, **15**, 12604–12627.
- 20 M. Schorb, I. Haberbosch, W. J. Hagen, Y. Schwab and D. N. Mastronarde, *Nat. Methods*, 2019, **16**, 471–477.
- 21 W. Li, K. G. Field and D. Morgan, *npj Comput. Mater.*, 2018, **4**, 36.
- 22 J. E. Salgado, S. Lerman, Z. Du, C. Xu and N. Abdolrahim, *npj Comput. Mater.*, 2023, **9**, 214.
- 23 N. J. Szymanski, C. J. Bartel, Y. Zeng, M. Diallo, H. Kim and G. Ceder, *npj Comput. Mater.*, 2023, **9**, 31.
- 24 H. Hysmith, E. Foadian, S. P. Padhy, S. V. Kalinin, R. G. Moore, O. S. Ovchinnikova and M. Ahmadi, *Digital Discovery*, 2024, **3**, 621–636.
- 25 A. Sinha, G. Ischia, G. Straffellini and S. Gialanella, *Ultramicroscopy*, 2021, **230**, 113365.
- 26 M. Ahmed, X. Guo and X.-M. Zhao, *Instrum. Sci. Technol.*, 2017, **45**, 659–682.
- 27 C. R. Dunnam, *Microsc. Today*, 1995, **3**, 30–31.
- 28 D. Chernoff, *Microsc. Today*, 1995, **3**, 30.
- 29 F. Salver-Disma, J.-M. Tarascon, C. Clinard and J.-N. Rouzaud, *Carbon*, 1999, **37**, 1941–1959.
- 30 M. Dutka and A. Prokhorova, *Microsc. Microanal.*, 2019, **25**, 554–555.
- 31 R. J. Henderikx, D. Mann, A. Domanska, J. Dong, S. Shahzad, B. Lak, A. Filopoulou, D. Ludig, M. Grininger, J. Momoh, *et al.*, *Biol. Crystallogr.*, 2024, **80**, 232–246.
- 32 K. Neselu, B. Wang, W. J. Rice, C. S. Potter, B. Carragher and E. Y. Chua, *J. Struct. Biol.*, 2023, **7**, 100085.
- 33 Y. Fei, B. Rendy, R. Kumar, O. Darts, H. P. Sahasrabudhe, M. J. McDermott, Z. Wang, N. J. Szymanski, L. N. Walters, D. Milsted *et al.*, *arXiv*, 2024, preprint, arXiv:2405.13930, DOI: [10.1039/D4DD00129J](https://doi.org/10.1039/D4DD00129J).
- 34 C. A. Schneider, W. S. Rasband and K. W. Eliceiri, *Nat. Methods*, 2012, **9**, 671–675.
- 35 L. N. Walters, Y. Fei, B. Rendy, X. Yang, M. Diallo, K. Jun, G. Wei, M. J. McDermott, A. Giunto, T. Mishra, *et al.*, *arXiv*, 2025, preprint, arXiv:2501.03165, DOI: [10.48550/arXiv.2501.03165](https://doi.org/10.48550/arXiv.2501.03165).
- 36 J. Postel, User datagram protocol, *Information Sciences Institute Technical report*, 1980.
- 37 M. Sim, M. G. Vakili, F. Strieth-Kalthoff, H. Hao, R. J. Hickman, S. Miret, S. Pablo-García and A. Aspuru-Guzik, *Matter*, 2024, **7**, 2959–2977.
- 38 F. Rahmanian, J. Flowers, D. Guevarra, M. Richter, M. Fichtner, P. Donnelly, J. M. Gregoire and H. S. Stein, *Adv. Mater. Interfaces*, 2022, **9**, 2101987.
- 39 X. Mu, C. Gillman, C. Nguyen and T. Gonen, *Annu. Rev. Biochem.*, 2021, **90**, 431–450.
- 40 D. B. Williams, C. B. Carter, D. B. Williams and C. B. Carter, *The transmission electron microscope*, Springer, 1996.
- 41 B. Michen, C. Geers, D. Vanhecke, C. Endes, B. Rothen-Rutishauser, S. Balog and A. Petri-Fink, *Sci. Rep.*, 2015, **5**, 9793.
- 42 M. Majumder, C. S. Rendall, J. A. Eukel, J. Y. Wang, N. Behabtu, C. L. Pint, T.-Y. Liu, A. W. Orbaek, F. Mirri, J. Nam, *et al.*, *J. Phys. Chem. B*, 2012, **116**, 6536–6542.
- 43 S. V. Kalinin, M. Ziatdinov, M. Ahmadi, A. Ghosh, K. Roccapiore, Y. Liu and R. K. Vasudevan, *Applied Physics Reviews*, 2024, **11**, 1–18.
- 44 H. Kim, J. Han and T. Y.-J. Han, *Nanoscale*, 2020, **12**, 19461–19469.
- 45 W. Yang, Z. Wang, T. Yang, L. He, X. Song, Y. Liu and L. Chen, *ACS Appl. Mater. Interfaces*, 2021, **13**, 53439–53453.

